




Effects of SiC particles codeposition and ultrasound agitation on the electrocrystallisation of nickel-based composite coatings

S. Pinate¹, F. Eriksson², P. Leisner¹, and C. Zanella^{1,3,*} 

¹Department of Materials and Manufacturing, School of Engineering, Jönköping University, Jönköping, Sweden

²Thin Film Physics Division, Department of Physics, Chemistry and Biology (IFM), Linköping University, Linköping, Sweden

³Department of Industrial Engineering, Trento University, Trento, Italy

Received: 9 April 2021

Accepted: 28 August 2021

Published online:

9 September 2021

© The Author(s) 2021

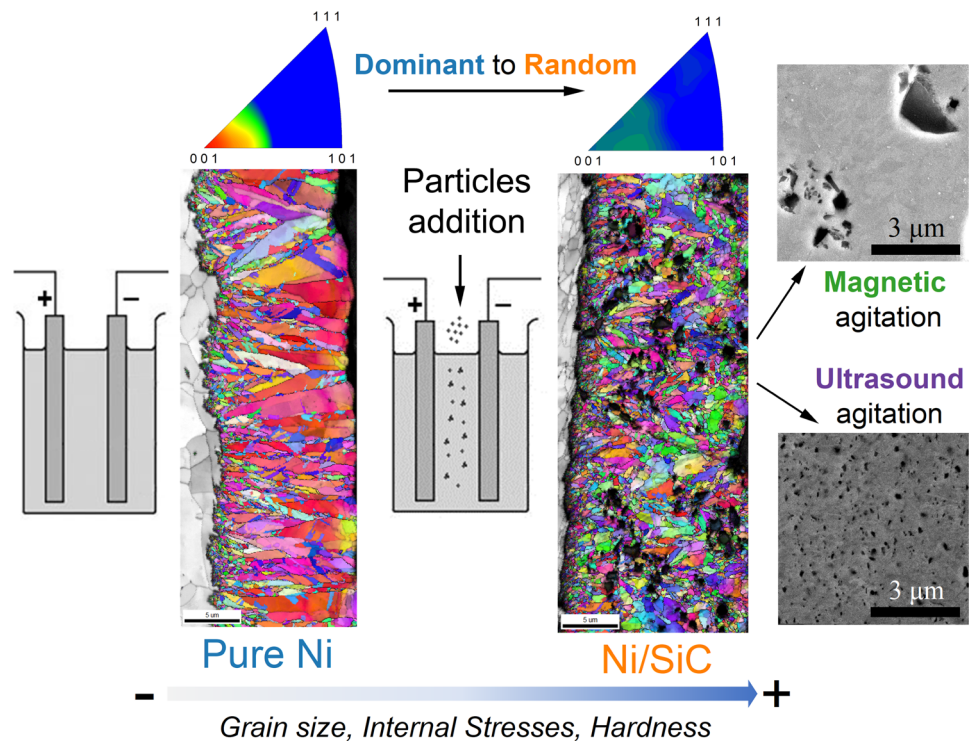
ABSTRACT

This study analysed the influence of the codeposition of SiC particles with different sizes: 50 nm, 500 nm and 5 µm, and the type of bath agitation (stirring or ultrasonic) on the electrocrystallisation of nickel coatings. The composites matrix microstructure was analysed by means of SEM, EBSD and XRD, to evaluate the grain size, crystal orientation, and internal stresses and was benchmarked against pure nickel samples electrodeposited in equivalent conditions. The codeposition of nano- and microsize particles with an approximate content of 0.8 and 4 vol.%, respectively, caused only a minor grain refinement and did not vary the dominant < 100 > crystal orientation observed in pure Ni. The internal stress was, however, increased by particles codeposition, up to 104 MPa by nanoparticles and 57 MPa by microparticles, compared to the values observed in pure nickel (41 MPa). The higher codeposition rate (11 vol.%) obtained by the addition of submicron-size particles caused a change in the grain growth from columnar to equiaxial, resulting in deposits with a fully random crystal orientation and pronounced grain refinement. The internal stress was also increased by 800% compared to pure nickel. The ultrasound (US) agitation during the deposition caused grain refinement and a selective particle inclusion prompting a decrease in the content of the particles with the larger particles. The deposits produced under US agitation showed an increase in the internal stresses, with double values compared to stirring. The increase in the deposits microhardness, from 280 HV in pure Ni to 560 HV in Ni/SiC submicron-US, was linked to the microstructural changes and particles content.

Handling Editor: Yaroslava Yingling.

Address correspondence to E-mail: caterina.zanella@ju.se; caterina.zanella@unitn.it
E-mail Addresses: santiago.pinate@ju.se; fredrik.eriksson@liu.se; peter.leisner@ju.se

GRAPHICAL ABSTRACT



Introduction

The protection of the surface provided by electrodeposited composite coatings against wear or corrosion is directly dependent on the characteristics of the matrix and the reinforcer phase but also by the deposition parameters. Typically the second phase is in the form of particles, which are themselves highly influenced by the production process [1, 2]. Composite layers can be controlled by the deposition parameters, e.g. electric current, bath chemistry, and cell geometry, particles load. In choosing the composite, metals with high corrosion resistance, such as nickel or nickel alloys, are desired as the matrix material, whereas hard particles are opted as the reinforcer phase, enhancing the composites' wear resistance [3, 4].

The role of the input parameters and their influence on the electrocrystallisation of pure metals, therefore on their microstructure and mechanical

properties, is well established [5]. However, there is a gap of knowledge obtained with pure metal systems to those with particles. The interactions between input variables might be modified due to the addition of particles to the electrolyte, causing complex and not well-understood interlinked effects between parameters [6], resulting in unpredictable changes in the electrodeposition of composites and their properties. Furthermore, the incorporation of particles into the deposit can also be affected, leading to a lack of process control.

In order to develop a production process where the properties of the composite coating are predictable, it is necessary to both understand the mechanisms of particles codeposition, which has been extensively studied in the last decades, and also understand how particles codeposition affects the matrix microstructure. The size, content, and distribution of particles codeposited within the matrix are the commonly the studied output in composites coatings research, but the mechanical performance of the composite

material is also dependant on the resulting metal microstructure, which might be affected by the incorporation of particles [7–10]. Thus, it is critical to understand the synergistic effect between metal electrocrystallisation and particles codeposition in order to link the grain size and the dispersion strengthening.

Multiple studies have been carried out where the influence of particles was examined, showing, for instance, that indeed their incorporation changed the characteristics of the microstructure, i.e. changing the deposits texture, grain size or internal stresses particles [11–14]. However, the high dependency between parameters and sensitivity to changes in the operation parameters [15] hinder extracting common elements between studies and limits the possibility of highlighting the synergies between particle codeposition and metal microstructure explicitly.

The present study aimed to identify the changes in the nickel matrix microstructure due to the codeposition of SiC particles. The microstructure of the Ni matrix was analysed when deposited in the presence of SiC particles with different sizes: 50 nm, 500 nm and 5 μm , and benchmarked against pure nickel samples produced under exact conditions. The agitation of the bath was done under stirring with a rotating magnet or under ultrasounds (US). The latter was used for better particles dispersion [16]. The electrodeposition was carried out in an additive-free Watts bath [17] with a particles load of 20 g L⁻¹. Amblard et al. [18] and Reddy [19] stressed the importance of bath chemistry in the development of inhibiting species on the cathode surface that promotes specific crystal growth directions changing the nickel electrocrystallisation. Therefore, the bath chemistry was kept additive-free, to avoid any possible impact from surfactants [20, 21]. This allowed a systematic investigation of the resulting microstructure, including internal stress, grain size, and texture as indicators of the electrocrystallisation conditions under the presence of SiC particles alone, and correlate their effect to the microhardness analysis of the deposits. Also, cathodic polarisation tests carried out in a solution without metal ions were used to assess the particles' influence in the hydrogen evolution reaction.

Experimental and characterisation details

Electrolyte composition and experimental set-up

Four specimens for each condition were electrodeposited by direct current (DC) at 4 A dm⁻² for 30 min ($\approx 24.5 \mu\text{m}$ thickness) from an additive-free Watts bath on low carbon steel plates, with a cathodic area of 3 cm by 5 cm. The electrolyte composition and process parameters are listed in Table 1. An external power source was used to provide the required conditions for the deposition process. The electrodeposition was performed in a thermally controlled cell (45 °C) with 500 mL bath volume and with parallel vertical electrodes configuration with a distance between electrodes of cathode and anode of 7 cm. Before electroplating, the steel substrate was mechanically ground with SiC grade #1000, cleaned ultrasonically in an alkaline soap and activated by pickling for 8 min in 2.5 M H₂SO₄. The pH of the electrolyte was set at pH 3.0 before deposition, and the pH was remeasured after producing each sample and adjusted by adding sulphuric acid or sodium hydroxide.

Composite coatings were produced adding 20 g L⁻¹ of SiC powder with different average size: SiC powder of nano- (gnm© #SiC-110 spherical β -SiC 50 nm), submicron- (gnm© #SiC-110 irregular angular-shaped β -SiC 500 nm), and microsize (H.C. Starck© SiC grade UF-05 irregular angular-shaped α -SiC 5 μm). In all conditions, the bath suspension was stirred for 12 h and agitated with ultrasound (US) for 30 min before electroplating. The stirring was applied continuously to maintain the powder in suspension. The electroplating was performed under two different agitation conditions: stirring at 200 rpm by a cylindrical-shaped magnetic rotator (0.7 cm diameter and 6 cm in length) placed at the bottom of the cell, or by an ultrasonic (US) probe (2 cm diameter and 5.5 cm in length) immersed 3 cm in the electrolyte and positioned vertically between the electrodes (Hielscher, 24 kHz, 0.087 W cm⁻³). In order to address the heating effect of the ultrasounds, a thermocouple was placed on the substrate, and the bath temperature was adjusted accordingly to maintain the substrate temperature constant and comparable to the stirred condition (45 °C).

The data of pure Ni deposited using stirring [22] from a previous study were included as a

Table 1 Plating bath composition and parameters

NiSO ₄ ·7H ₂ O	240 g L ⁻¹	Particle concentration	20 g L ⁻¹
NiCl ₂ ·6H ₂ O	45 g L ⁻¹	SiC particle size	50 nm, 500 nm, 5 μm
H ₃ BO ₃	30 g L ⁻¹	Current	DC; 4 A dm ⁻²
pH	3.0	Deposition time	30 min
Temperature	45 °C	Stirring speed	200 rpm
Anode	Ni sheet;	Ultrasonic agitation	24 kHz; 0.087 W cm ⁻³

benchmark. The data from Ni/SiC50 and Ni/SiC500 under magnetic stirring were also extracted from a previous study [23]. All samples were produced under the exact conditions as described in Table 1.

The current efficiency (CE) of the process was calculated by comparing the theoretical deposited mass calculated by Faraday's law of electrolysis to the experimental deposited metallic mass minus the particles' mass (as measured by WDS).

Polarisation test

The hydrogen evolution reactions (HER) were analysed by potentiodynamic polarisation curves generated in a solution with similar conditions: pH, temperature, conductivity and geometry as the electrodeposition bath. The composition of the solution is the same as the deposition bath but without the metal salts to permit the analysis of the influence of particles in the HER. The pH of the solution was adjusted to 3.0 and polarisation was applied from OCP to cathodic overvoltage equivalent to a current density of 5 A dm⁻². An Ag/AgCl (3 M KCl) reference electrode and a platinum electrode were used as reference and counter electrode, while the working electrode was the same steel substrate as for the deposition. An IVIUM Vertex potentiostat was used for the electrochemical measurements, and the sweep rate was 2 mV s⁻¹.

Coating characterisation

The characterisation of the coatings was carried out in the same area for all samples, thus minimising possible differences resulting from the fluid dynamics or current distribution. The analyses were done in the centre of the sample in order to avoid an edge effect resulting from the current density distribution. Furthermore, the area of interest was distanced 1.5 cm away from the rotating magnet and about 4 cm away from the US probe's tip to avoid a shielding effect during electrodeposition.

The quantification of Si was performed by wavelength-dispersive X-ray spectroscopy (WDS, EDAX-TSL) due to the better resolution in the measurement of light elements at low content compared to energy-dispersive spectroscopy (EDS). The content of SiC in the composites was calculated based on Si pure standards and under the assumption that the SiC powders have a stoichiometric composition. The analysis of weight% for the standard and each sample was performed using an acceleration voltage of 10 kV and beam current ranging from 14.5 to 18 nA. The volume content of SiC was expressed as the average value of five different WDS area measurements considering a density of 3.22 g cm⁻³ at 25 °C.

The surface morphology was observed by scanning electron microscopy (SEM, JEOL 7001F). Phase analysis was performed using X-ray diffraction (XRD) on a Panalytical X'pert diffractometer using a Cu X-ray tube, a Bragg–Brentano HD optics with a 1/2° divergence slit and a 1/2° anti-scatter slit on the incident side, and a 5 mm anti-scatter slit and an X'celerator detector in scanning line mode on the secondary side.

Samples were prepared in cross section by mechanical polishing and analysed by electron backscattered diffraction (EBSD, EDAX-TSL). The analysis was performed on two samples for each condition with an electron probe current of 4.4 nA at an acceleration voltage of 15 kV. A step size of 80 nm was used to build the EBSD maps, and the analysis was carried out in the growth direction by the OIM 5TM, disregarding all data points with coefficient index (CI) < 0.1. A grain was defined as a region consisting of at least three similarly oriented connected points with a less than 10° misorientation and the grain size by the number of points in the region. The grain area average was calculated by weighting the value of the area fraction of each grain, and the grain diameter was calculated from the averaged grain area and considering it a circle. Twin boundaries were excluded from the calculations of the grain size.

The microhardness of the deposits was measured on cross section by Vickers indenter (NanoTest™ Vantage) with an indentation load of 100 mN and a dwell time of 10 s. Thirty repetitions were done on two samples of each condition, and the hardness was expressed as the average.

Internal stress measurements were performed using the $\sin^2\psi$ -technique using a five-axis cradle on a Panalytical Empyrean diffractometer. The diffractometer was used in a parallel beam configuration with a point-focused copper anode source (Cu K α , $\lambda = 0.154$ nm), operating at 45 kV and 40 mA. The primary beam was conditioned by an X-ray lens and 2×2 mm² crossed-slits, and in the secondary beam path, a 0.27° parallel plate collimator was used. A PIXcel detector was used in 0D mode for the data acquisition. θ - 2θ measurements were performed in a range of 4° around the 400 reflections of Ni for different tilt angles ψ , with $\sin^2\psi$ in the range of 0–0.9. The d-spacing was calculated and plotted as a function of $\sin^2\psi$, and the residual stress was calculated from the slope using Young's modulus ($E = 225.13$ GPa) and Poisson's ratio ($\nu = 0.2956$) for Ni. The internal stress analysis was performed using Panalyticals X'Pert Stress software.

Results and discussion

Electrodeposition

The increase in pH after electrodeposition (Fig. 1) showed that the metal reduction was accompanied by hydrogen evolution reactions (HER) [18]. The faradaic current was partially used in the side reaction, decreasing also the current efficiency (CE) of the process. The presence of particles prompted a slight increase in the hydrogen reduction, observed by the changes of pH after electrodeposition, causing a minor loss of CE in all composites compared to pure Ni. The US agitation also further increased hydrogen evolution, increasing the pH deviation (ΔpH) compared to stirring. During the cathodic reaction, H^+ is consumed along with the Ni ions at the cathode surface. The US promoted a continuous replenishment of these ions due to the more vigorous agitation than stirring, encouraging hydrogen evolution. Furthermore, Coleman et al. [24] observed variations in the electrode potential, in addition to the increase in mass transfer of ions, after immersing a US horn directly into the bath for agitation. Therefore, a shift in the reduction potential resulting from ultrasounds might have prompted hydrogen reduction instead of Ni^{2+} , causing a decrease in CE for all processes under US agitation, where CE loss was more evident in the deposition of Ni/SiC500. For instance, the CE was around 95% under stirring, while using US agitation, the CE dropped down to about 90%. Nevertheless, the CE of the processes was in agreement with the literature, as the cathode efficiency for Watts baths generally remains between 90 and 97% [25].

The polarisation curves of particles in suspension (Fig. 2) also confirmed the influence of the particles on the reduction in H^+ . The curve of the solution without particles (black-coloured) showed an initial current plateau, which corresponded to the HER of the H^+ available in the solution at pH 3, the water hydrolysis coincided with the curve at lower potential values after the plateau. The addition of particles promoted an initial shift in the current density to reduce the free H^+ , thus encouraging a higher reduction rate. The shift was more pronounced in the solution with SiC500. The part of the curve that represented the water hydrolysis for the solutions with SiC50 and SiC5 was comparable to the solution (water at pH 3.0) at plating condition. In the solution with SiC500 the curve was displaced, showing the

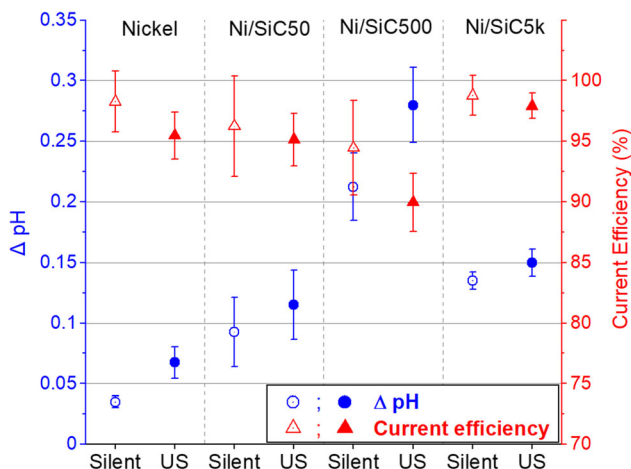


Figure 1 pH variation (ΔpH) after electrodeposition and current efficiency (%) of the process, both displayed as averages of four experiments for each condition.

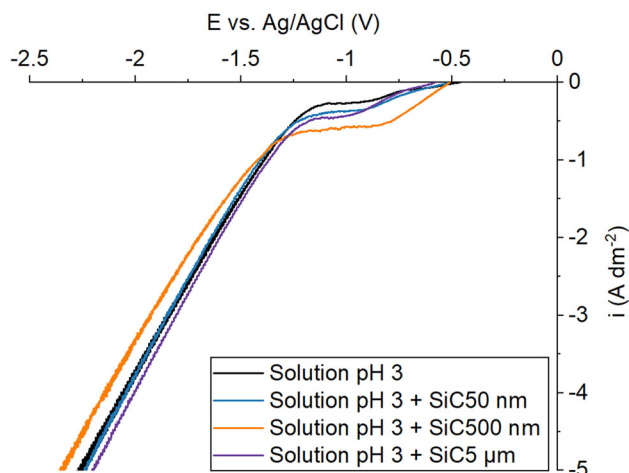


Figure 2 Polarisation curves of a solution without Ni ions at pH 3.0 with and without particles.

influence of the particle over the HER. A previous study [23] showed the buffering capability of these particles by titrating a solution with particles, starting from pH 3.0, with NaOH as titrator. The solution (water, pH = 3.0) without particles showed a shift in pH as the titrator was added, whereas in the solution with particles, the pH change was slower or did not occur, in the case of the SiC500. It was presumed that the additional effect in the H^+ reduction caused by the presence of non-inert SiC particles was recorded by the polarisation tests.

The Ni/SiC composites were produced from the solution as listed in Table 1. The codeposition rate of SiC particles is reported in Table 2. The codeposition fraction varied between the particle sizes. As often reported in the literature, the codeposition of nanoparticles was low, close to 1 vol.% content [8, 26–28], in comparison to larger sizes [26, 27, 29, 30], while in the case of the submicron (SiC500) and microparticles (SiC5k) the inclusion rate value was around 11 vol.% and 4 vol.%, respectively.

Under US agitation, the codeposition of SiC50 was increased from ≈ 0.8 to ≈ 2.6 vol.%. Similar effects were reported in previous studies with nanoparticles [31, 32], where their content was increased. US agitation kept more effectively the nanosize particles in a

closer range to the cathode surface than the stirring, thus increasing their chance to be embedded by the metal growth, thereby increasing the codeposition rate. However, the codeposition of SiC500 and SiC5 was decreased by about 60% and 70%, respectively, compared to stirring. This was due to the high energy of the ultrasonic waves, as well as cavitation near the cathode, which affected the codeposition of larger particles negatively. Due to the system set-up with the US probe immersed in the cell, the high energy was directly released in the electrolytic bath. The surface cathode remains unshielded and exposed to cavitation. This may have caused the larger particles to collide and 'bounce' away from the electrode or be removed from the surface by the cavitation before being anchored by the growing metal [33]. Figure 3a, c shows a broad particle size distribution in SiC500, ranging from smaller than 500 nm to microsized. The particle entrapment happened as clusters of particles within the matrix. Under US agitation, the dispersion was improved, and particles were entrapped almost entirely across the metal (Fig. 3b). However, SiC500 particle size distribution seemed to have narrowed, and codeposited particles appear to be smaller than 500 nm in size (Fig. 3d). Essentially, US agitation promoted a selective entrapment encouraging only the codeposition of the smaller and more dispersed particles. As a consequence of repelling the larger particles, which would represent a sizeable fraction of the total volume, the codeposition of SiC was decreased by the US agitation (Table 2). Compared to stirring (Fig. 3a), US agitation might have increased the total number of particles (Fig. 3b).

Microstructure and internal stresses

The XRD spectra showed six visible diffraction peaks for all conditions: (111), (200), (220), (311), (222) and (400). The relative texture coefficient, RTC, was calculated [34] for the texture quantification of the deposits using these six crystal planes. The relative texture coefficient for a (hkl) crystal plane was defined as:

Table 2 Codeposited SiC weight and volume content (%) as determined by WDS

	SiC50		SiC500		SiC5k	
	Sil	US	Sil	US	Sil	US
Vol.%	0.78 ± 0.13	2.81 ± 0.58	11.18 ± 1.15	4.56 ± 0.17	3.84 ± 0.25	1.09 ± 0.17
Wt.%	0.28 ± 0.05	1.04 ± 0.16	4.34 ± 0.48	1.70 ± 0.07	1.42 ± 0.10	0.39 ± 0.06

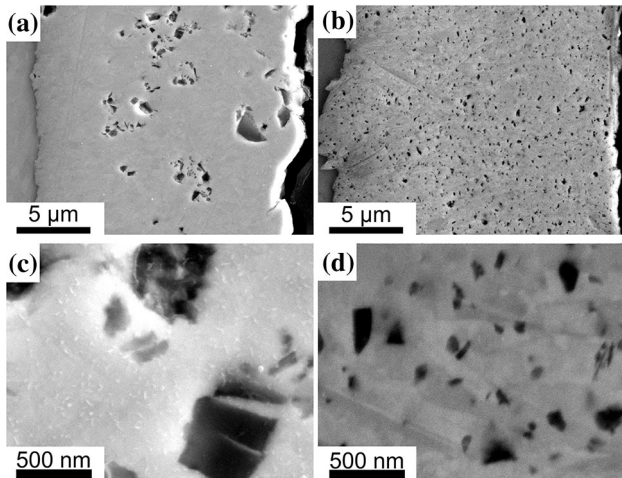


Figure 3 SEM cross section image of Ni/SiC 500 composites produced using **a** stirring and **b** US, and high magnification images of the particles using **c** stirring and **d** US.

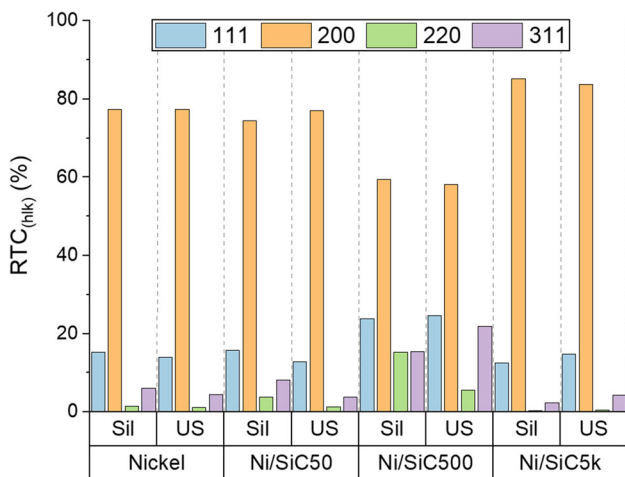


Figure 4 $RTC_{(hkl)}$ determined for the different orientations related to the crystal planes observed in electrodeposited coatings under different agitations. The RTC values for (200) and (400) as well as (111) and (222) are shown as a single hkl value.

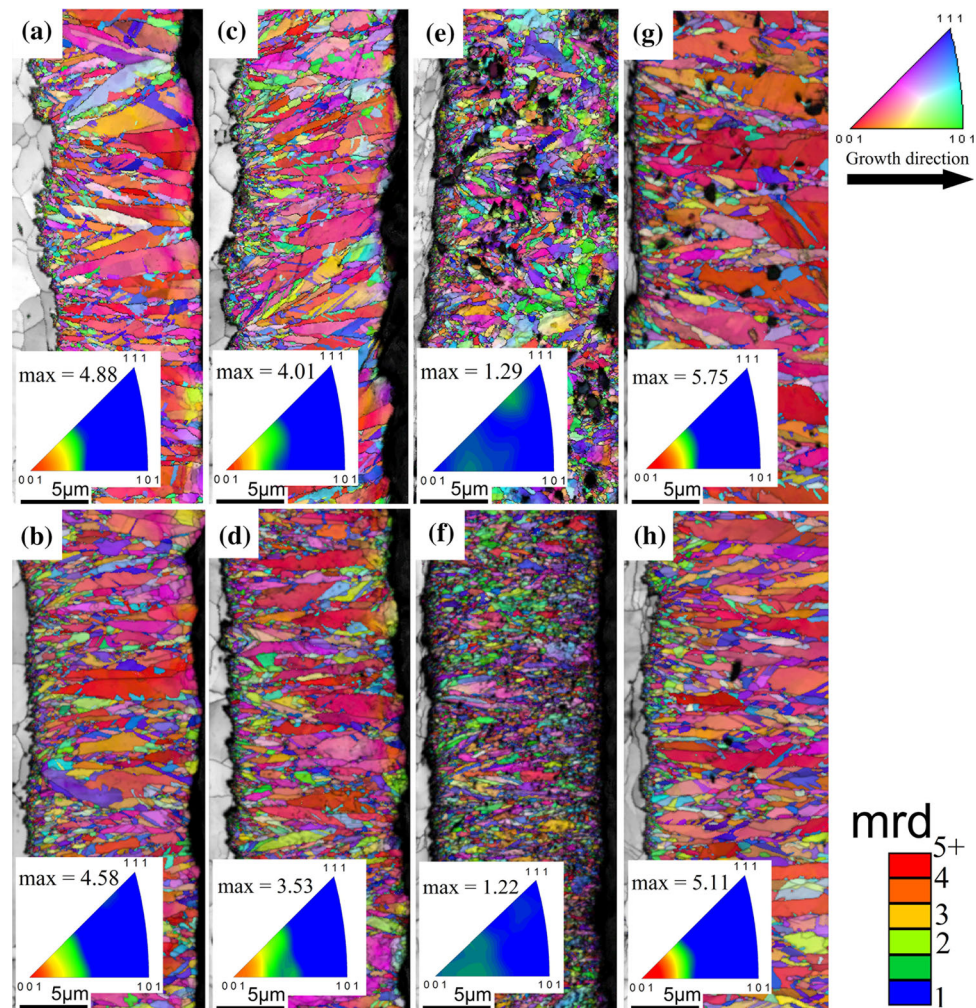
$$RTC_{(hkl)}(\%) = 100 \times \frac{I_{(hkl)}/I_{(hkl),P}}{\sum_1^n I_{(hkl)}/I_{(hkl),P}} \quad (1)$$

where $I_{(hkl)}$ is the intensity of the reflection for the (hkl) crystal plane in the analysed sample and $I_{(hkl), P}$ is the intensity of the reflection for the same crystal plane in a standard Ni powder sample with random orientation.

Figure 4 shows the $RTC_{(hkl)}$ of the deposits, where the linearly dependent lattice planes, e.g. (200) and (400), and (111) and (222), are shown as a single hkl -value. Pure nickel, Ni/SiC50 and Ni/SiC5k showed textured microstructures with (200) crystal plane preference, typical of the so-called free mode crystal growth under the potential electrical field [18]. In the Ni/SiC5k deposits, the intensity of the (200) crystal plane was higher than in the pure Ni deposits (Fig. 4), presumably due to the larger grains of the matrix, observable in Ni/SiC5k (Fig. 5g, h) compared to pure Ni (Fig. 5a, b). These observations were supported by the larger crystallite sizes measured in Ni/SiC5k, 612 Å (stirring) and 602 Å (US), compared to pure Ni, 487 Å and 480 Å, respectively.

The codeposition of SiC500 under stirring caused a change in the nickel electrocrystallisation. The deposit $RTC_{(hkl)}$ showed a decrease in the (200) intensity and enhanced quality in the rest of the directions, while under US agitation, the $RTC_{(hkl)}$ of SiC500 showed a decrease in the (220) plane and an increase in the (311). A mix $< 100 + 211 >$ preferred orientation was apparent in the SiC500 deposits independently of the agitation type, as evidenced by the intensity of the (200) crystal plane and the enhancement of (111) and (311), attributed to a dispersed $< 211 >$ orientation [13]. Similar changes in nickel crystals were observed in previous studies [13, 27, 35], where the enhancement of the $< 211 >$ mode of crystal growth was associated with the presence of particles. An adsorption–desorption phenomenon of H^+ on the particles surface [23, 27, 36] could have altered the pH in the vicinity of the cathode, prompting the $< 211 >$ crystal growth, which is associated with the presence of nickel hydroxide in the electrodeposition of nickel [18]. Tudela et al. [37] also observed in additive-free nickel deposits a more dominant $< 211 >$ orientation as the result of an increased inhibition effect by $Ni(OH)_2$, identifying as well an inverse relationship where the ‘free’ (100) growth mode was reduced in favour of the $< 211 >$ intensity. In essence, such inhibition effect on the free (100) growth mode reduces its intensity while (111) and (311) crystal planes, i.e. $< 211 >$, are promoted, and thus modifying the preferred orientation of the deposit, as suggested by the data in Fig. 4. Furthermore, the accompanying changes in pH as the result of US agitation (Fig. 1) might have caused a further encouragement of the $< 211 >$ mode of crystal

Figure 5 Orientation map, colour-coded in relation to the electrodeposits' growth direction, shown by an arrow in the legend with the corresponding inverse pole figure, including the max texture intensity in units of multiplies of random distribution (mrd) as indicated by the colour bar. **a** Ni Sil **b** Ni US **c** Ni/SiC50 Sil **d** Ni/SiC50 US **e** Ni/SiC500 Sil **f** Ni/SiC500 US **g** Ni/SiC5k Sil **h** Ni/SiC5k US.



growth, as observed by the increase in the intensity in the (311) direction, visible in Ni/SiC500-US (Fig. 4).

The results obtained by the electron backscatter diffraction (EBSD) were in agreement with the XRD line profile analysis and gave an insight into the anisotropy of the grains that tend to grow as columnar structures perpendicular to the surface. Figure 5 shows the EBSD maps of cross sections and the corresponding inverse pole figures for each deposition conditions. The inverse pole figures confirmed the preferred $\langle 100 \rangle$ crystal direction, except for Ni/SiC500 (Fig. 5e, f), where a random texture was observed. As previously discussed, the increase in inhibition by US agitation or SiC codeposition slightly decreased the max texture intensity of the $\langle 100 \rangle$ by promoting growth inhibition.

From the EBSD maps, a grain size distribution in relation to the area fraction and the weighted grain size average were calculated and are reported in

Fig. 6. Pure nickel (Fig. 5a) and Ni/SiC5k (Fig. 5g) showed a comparable columnar growth; however, it is of interest to note that the grain sizes deduced by the EBSD data were in slight disagreement with the crystallite sizes estimated by XRD. In the case of the latter, the data showed that Ni/SiC5k had larger grains compared to pure Ni, while from the EBSD data, the microstructure of both was equivalent (Fig. 6). Lampke et al. [38] also observed similarities between the microstructure of pure Ni and Ni/SiC5k; in their study, similar intercept values: normal to growth and in growth direction were observed despite the addition of 5 μm particles (0.49 ± 0.47 and 0.68 ± 0.73 in pure Ni and 0.51 ± 0.26 and 0.66 ± 0.92 in Ni/SiC5k). The columnar growth was preserved, and the grain size distribution was virtually unaltered by the US agitation in both pure Ni and Ni/SiC5k, although it was possible to notice a slight increase in the fraction of smaller grains.

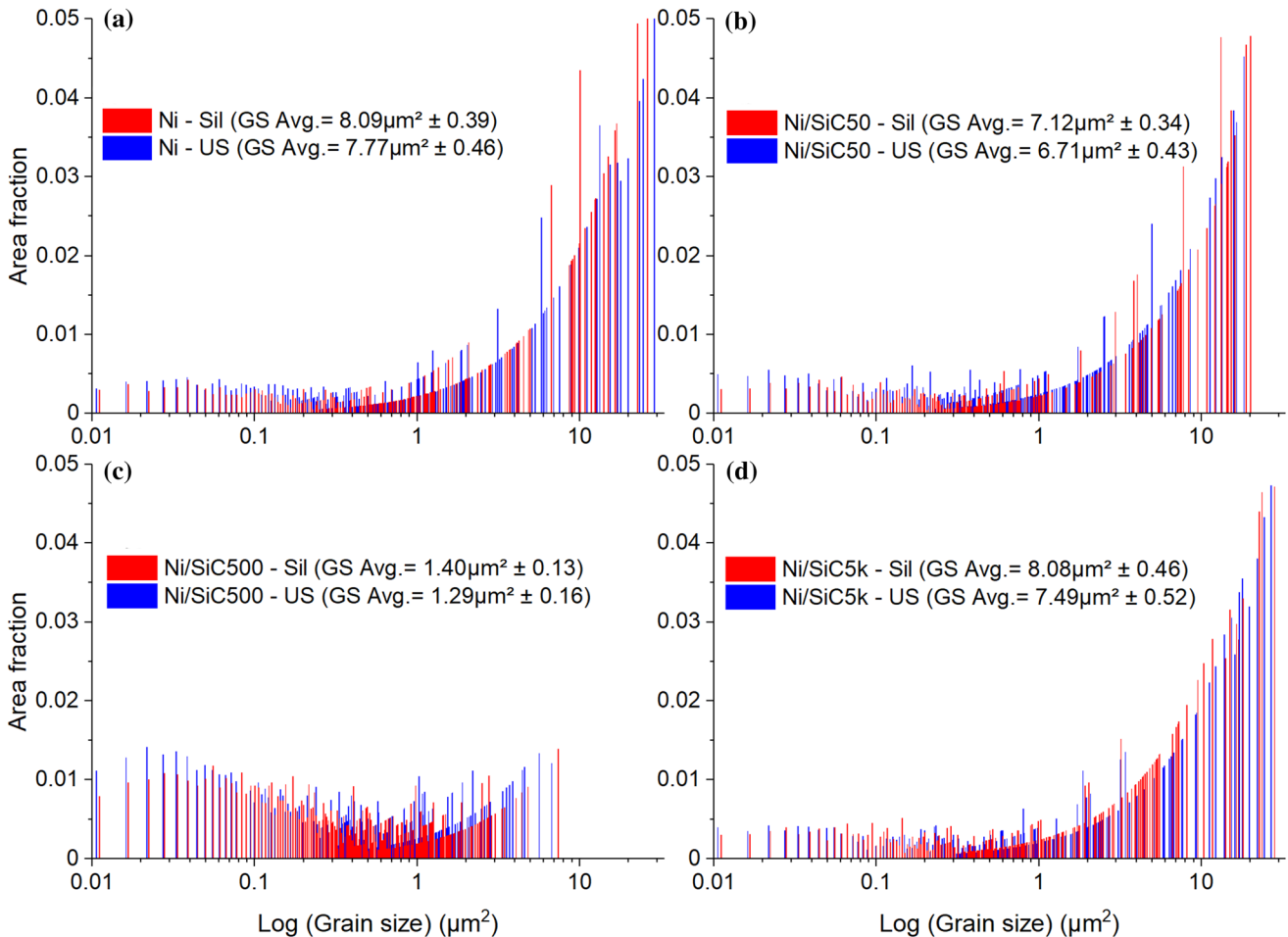


Figure 6 Distribution of the grain size (μm^2) in relation to the area fraction. **a** Pure Ni **b** Ni/SiC50 **c** Ni/SiC500 **d** Ni/SiC5k.

Tudela et al. [37] also reported an increase in smaller grains in between the larger columnar crystal under US.

The addition of SiC50, when using stirring or US agitation, induced some changes in the microstructure, without affecting the columnar growth. The addition of particles modified the electrocrystallisation, effectively reducing grains with an area higher than $10 \mu\text{m}^2$ (Fig. 6b), favouring an increase in smaller grains. The codeposition of SiC50 revealed a relationship between content, grain size, and nucleation rate. The particles promoted nucleation over growth, promoting grain refinement. Nevertheless, due to the low content of particles, this effect in the Ni/SiC50 using stirring was diminished. The increase in codeposition by US agitation, from ≈ 0.8 vol.% using stirring up to 2.8 vol.%, promoted further grain refinement ($\approx 6.7 \mu\text{m}^2$), in addition to the refinement initiated by the US agitation itself, as observed in pure Ni.

The effect on the metal electrocrystallisation was evident in Ni/SiC500 samples with no major differences between the two types of agitation. The increased nucleation due to the codeposition of SiC particles resulted in a pronounced grain refinement (Fig. 6c). In both agitation modes, the grain area with less than $1 \mu\text{m}^2$ represented most of the total area. Furthermore, the grain morphology changed from columnar to equiaxial (Fig. 5e, f), with a higher number of randomly oriented grains. Therefore, combined with the increase in HER, Ni/SiC500 deposits were randomly oriented as previously discussed.

Figure 7 shows the surface topography of pure Ni and Ni/SiC500 both using stirring and US agitation. A pyramidal-shaped surface topography was observed for pure Ni using stirring (Fig. 7a). Under US agitation, the pyramidal shape was maintained with a negligible change in size (Fig. 7b). In Ni/SiC500 (Fig. 7c), the surface topography was

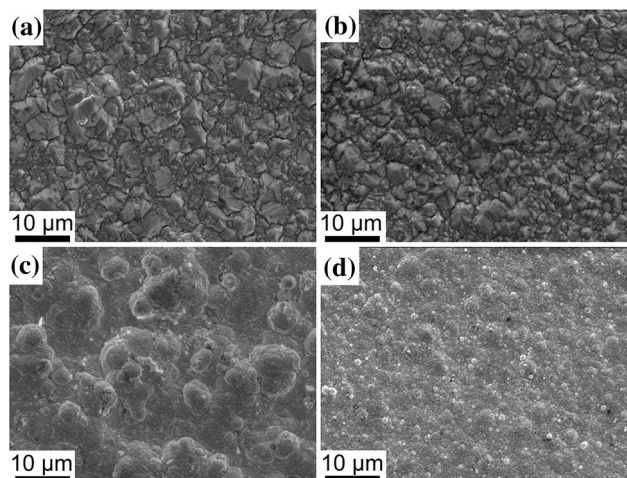


Figure 7 SEM image of surface topography: **a** Pure Ni—stirring **b** Pure Ni—US **c** Ni/SiC500—stirring **d** Ni/SiC500—US.

modified to globular-shaped structures. The size of the surface globularity was reduced (Fig. 7d), thus showing the effect of grain refinement. In previous studies, refinement was also observed under US agitation [16, 31, 32, 39]. Winand [40] extended the concept of inhibited growth in the analysis of electrodeposited microstructure. Columnar growth, bidimensional nucleation is substituted by tridimensional nucleation, globular growth, at higher inhibition. Similar to the structures reported in this study, Pavlatou et al. [27] also observed pyramidal-shaped surface structures dominated by (100) texture, in uninhibited, nickel deposits, while nickel deposits dominated by the (111) crystal orientation, resulted in globular-shaped surface structures.

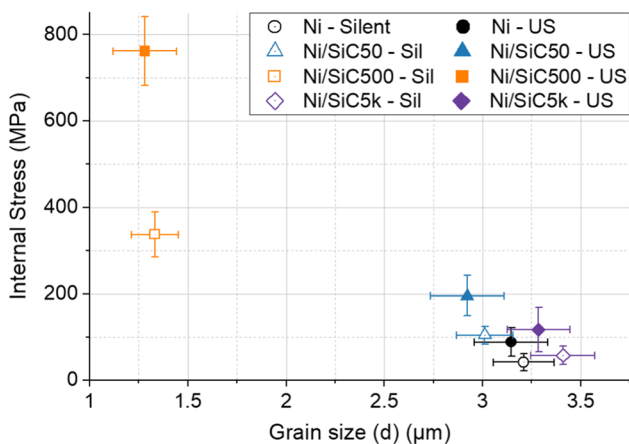


Figure 8 Internal stress (MPa) versus grain size diameter (μm) measured for the electrodeposits under agitation by stirring and US.

The internal stresses extracted from the XRD profiles are correlated to the deposits grain size in Fig. 8. In agreement with Godon et al. [41], the higher stress values were associated with smaller grain sizes. Two mechanisms modified the electrocrystallisation of the metal, causing grain refinement: particle codeposition and US agitation. Codeposition of nanosize and submicron particles caused an increase in internal stresses. Ni/SiC5k showed similar internal stress values compared to pure Ni, although SiC content was around 4 vol.%, proving that only the smaller-sized particles modify the metal electrocrystallisation.

US agitation also promoted grain refinement. However, in all deposits under US, the internal stress values were doubled compared to stirring, even if the grain sizes were not affected. Prasad et al. [42] observed the opposite effect. However, the authors reported a change in the hydrogen evolution with pH 4 as plating condition, a reduction in incorporation of atomic hydrogen in the deposit led to lower internal stresses. Nevertheless, in the present study US agitation promoted in all cases, an increase in HER at a lower plating pH. The inverse pole figures (Fig. 5) showed a decrease in the maximum of intensity, thus indicating inhibition. Consequently, the internal stresses were increased by the changes in the electrocrystallisation, i.e. grain refinement and texture, leading to the competition of fitting different than $\langle 100 \rangle$ growth directions within the metal deposit. Also, in the samples under magnetic stirring, where the microstructure was more random, the internal stresses were also higher. Godon et al. [41] also observed a relationship between lower internal stresses in deposits with larger grain sizes dominated by $\langle 100 \rangle$ crystal domain, and higher internal stresses in deposits with smaller grain sizes and dominated by random crystal orientations.

Microhardness

Microhardness tests revealed a relationship between microstructural changes (Fig. 9) and codeposition (Fig. 10), linked to the strengthening of the deposits. The changes in the metal electrocrystallisation, promoted by particles codeposition and US agitation, resulted in grain refinement, increased internal stresses, and changes in the crystalline orientation. Therefore, the total hardness of the composite resulted in a combination and contribution of different

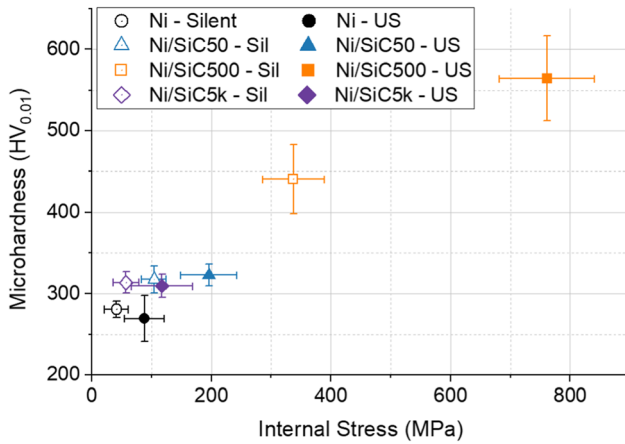


Figure 9 Microhardness (HV) versus internal stresses (MPa) measured for the electrodeposits under agitation by stirring (silent) and ultrasound (US).

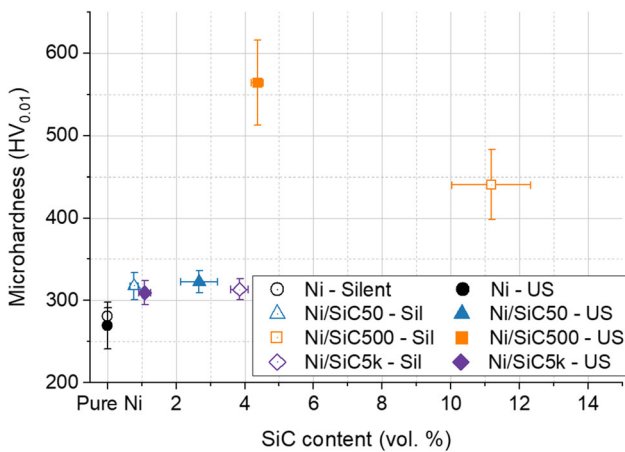


Figure 10 Microhardness (HV) versus codeposited SiC volume content (%) as determined by WDS, as well as pure nickel, under agitation by stirring (silent) and ultrasound (US).

strengthening effects. For instance, the decrease in grain size, i.e. the increase in grain boundaries, reinforced the metal by Hall–Petch strengthening mechanism [43], while particles deposition further strengthened the material by dispersion strengthening [43, 44]. Additionally, the material was also strengthened by the rise in internal stresses [41]. Furthermore, as demonstrated by Spanou and Pavlatou [45], the changes in the crystallographic orientation might have also influenced the final hardness of the deposits.

The pure nickel deposited by stirring had a hardness about 280 HV. US agitation did not introduce major changes in grain size, nor in internal stress. Therefore, the microhardness values were comparable between the two agitations modes (Fig. 9). In Ni/

SiC5k samples, only minor changes in the electrocrystallisation were observed of the metal by adding micro-size particles under stirring. Thus the increase in hardness values, compared to pure Ni, was due only to particle dispersion strengthening (Fig. 9). Although US agitation reduced the particle content, the hardness values remained somewhat similar to stirring. This was due to the changes in the electrocrystallisation by US, where the internal stresses increased. Therefore, the final hardness in Ni/SiC5k under the two agitation modes resulted in similar hardness values, where the higher internal stresses induced by the US agitation compensated for the loss of particle content.

Figure 9 shows a linear increase relationship between the increase in internal stress and microhardness. Even though the codeposition of SiC50 using stirring was minimal (0.8%), the slight changes in the metal electrocrystallisation, i.e. grain size and internal stress, caused an increase in hardness compared to pure Ni. Furthermore, the hardness value of Ni/SiC50 was somewhat similar to Ni/SiC5k, despite the higher micro-SiC content of the latter, due to the presence of larger grains and a more dominant < 100 > texture. Spanou and Pavlatou [45] also observed a lower microhardness in Ni/nano-TiO₂ deposits with < 100 > texture compared to a Ni matrix with < 110 > texture, regardless of particles incorporation rate, highlighting the importance of considering the effects of a given preferred orientation in hardness. The use of US agitation promoted an increase in SiC50 content (2.8 vol.%), internal stress and grain refinement. However, this was not translated into a significant change in microhardness compared to Ni/SiC50 using stirring, showing similar hardness values (Fig. 10).

The highest hardness in the samples produced by stirring was attained in the codeposition of SiC500 (440 HV), and US agitation led to a further increase (564 HV). Under the two agitation modes, Ni/SiC500 exhibited the synergies of a stronger grain refinement (Fig. 6), higher content of particles (Table 2), and an increase in the internal stresses compared to the other deposits (Fig. 9). The major changes in the Ni electrocrystallisation because of SiC500 codeposition led to changes in texture and microstructure, promoting changes in the grain morphology from columnar to somewhat equiaxial resulting in grain refinement, i.e. Hall–Petch strengthening. Which, combined with the increase in the internal stresses and dispersion

strengthening, improved the final hardness of the deposit (Fig. 10).

Ni/SiC500 under US agitation illustrates the importance of selecting a suitable production method. Although particle content was more than halved, and the grain size was comparable between the two agitation modes, an appropriate agitation method improved the dispersion of the particles (Fig. 3). Therefore, it favoured a further increase in hardness, albeit the lower particle volume content (Fig. 10).

Conclusions

The electrocrystallisation of the Ni matrix was influenced to different extents by particle codeposition and bath agitation mode. Multiple factors linked to the microstructural changes and particles reinforcement contributed to the hardness. This work proved that particle codeposition itself induces crystallisation changes evidencing that in the hardness of composite coatings, not only the particles content but also their synergistic effect over the electrocrystallisation process contribute to hardening.

The ultrasonic agitation promoted hydrogen evolution during deposition. The rise in the reduction in hydrogen was accompanied by a decrease in current efficiency and an increase in nickel growth inhibitors. Although the ultrasonic agitation had a minor impact on the deposits grain size, all samples under ultrasounds showed an increase in internal stress linked to the increase in hydrogen evolution.

Micro-size particles had a minor impact in the metal matrix microstructure showing similarities, e.g. grain size, texture and internal stress values to the pure nickel samples regardless of the type of agitation. Therefore, the improvement in hardness of the Ni/SiC5k deposits compared to pure Ni was due to particle strengthening by codeposited microparticles.

The changes induced by nanoparticles in the nickel microstructure: grain refinement, increase in internal stresses and changes in the crystallographic orientation, were sufficient to provoke hardening in Ni/SiC50 matching Ni/SiC5k microhardness values, albeit the low content of nanoSiC (≈ 0.8 vol.%) compared to micro (≈ 3.4 vol.%).

The synergistic effect between electrocrystallisation and SiC codeposition was more evident in Ni/SiC500 samples regardless of the agitation mode. The particle codeposition promoted significant changes in the

microstructure: high grain refinement and equiaxial-dominated nickel growth. Consequently, the internal stresses were increased, more than in other composites. Ni/SiC500 exhibited the synergies of more substantial grain refinement, higher content of particles and an increase in the internal stresses compared to the other deposits, resulting in deposits with high hardnesses.

Furthermore, the study of Ni/SiC500 under ultrasonic agitation revealed the more significant contribution to the hardness of the deposit caused by particle distribution than the one caused by the volume content. Although under ultrasounds, the particle content in Ni/SiC500 was more than halved compared to magnetic stirring, the combined effects of Hall–Petch strengthening, internal stress, particle-strengthening and better particle dispersion resulted in deposits with the highest hardness.

Funding

Open access funding provided by Jönköping University. The research was partially funded by the project FunDisCo (project reference number 20310117), supported by Knowledge Foundation, Sweden.

Declarations

Conflict of interest The authors declare that they have no conflict of interest.

Open Access This article is licensed under a Creative Commons Attribution 4.0 International License, which permits use, sharing, adaptation, distribution and reproduction in any medium or format, as long as you give appropriate credit to the original author(s) and the source, provide a link to the Creative Commons licence, and indicate if changes were made. The images or other third party material in this article are included in the article's Creative Commons licence, unless indicated otherwise in a credit line to the material. If material is not included in the article's Creative Commons licence and your intended use is not permitted by statutory regulation or exceeds the permitted use, you will need to obtain permission directly from the copyright holder. To view a copy of this licence, visit <http://creativecommons.org/licenses/by/4.0/>.

References

- [1] Low CTJ, Wills RGA, Walsh FC (2006) Electrodeposition of composite coatings containing nanoparticles in a metal deposit. *Surf Coat Technol* 201(1–2):371–383. <https://doi.org/10.1016/j.surfcoat.2005.11.123>
- [2] Kerr C, Barker D, Walsh F, Archer J (2000) The electrodeposition of composite coatings based on metal matrix-included particle deposits. *Trans IMF* 78(5):171–178. <https://doi.org/10.1080/00202967.2000.11871333>
- [3] Wang S, Ma C, Walsh FC (2020) Alternative tribological coatings to electrodeposited hard chromium: a critical review. *Trans IMF* 98(4):173–185. <https://doi.org/10.1080/00202967.2020.1776962>
- [4] Mahidashti Z, Aliofkhaezrai M, Lotfi N (2017) Review of nickel-based electrodeposited tribo-coatings. *Trans Indian Inst Met* 71(2):257–295. <https://doi.org/10.1007/s12666-017-1175-x>
- [5] Gamburg YD, Zangari G (2011) Theory and practice of metal electrodeposition. Springer Science+Business Media LLC, New York
- [6] Walsh FC, Wang S, Zhou N (2020) The electrodeposition of composite coatings: diversity, applications and challenges. *Curr Opin Electrochem* 20:8–19. <https://doi.org/10.1016/j.coelec.2020.01.011>
- [7] Spanou S, Pavlatou EA, Spyrellis N (2009) Ni/nano-TiO₂ composite electrodeposits: textural and structural modifications. *Electrochim Acta* 54(9):2547–2555. <https://doi.org/10.1016/j.electacta.2008.06.068>
- [8] Lampke T, Wielage B, Dietrich D, Leopold A (2006) Details of crystalline growth in co-deposited electroplated nickel films with hard (nano) particles. *Appl Surf Sci* 253(5):2399–2408. <https://doi.org/10.1016/j.apsusc.2006.04.060>
- [9] Ortolani M, Zanella C, Azanza Ricardo CL, Scardi P (2012) Elastic grain interaction in electrodeposited nanocomposite nickel matrix coatings. *Surf Coat Technol* 206(8–9):2499–2505. <https://doi.org/10.1016/j.surfcoat.2011.10.056>
- [10] Zanella C, Lekka M, Bonora PL (2009) Influence of the particle size on the mechanical and electrochemical behaviour of micro- and nano-nickel matrix composite coatings. *J Appl Electrochem* 39(1):31–38. <https://doi.org/10.1007/s10800-008-9635-y>
- [11] Góral A (2017) Nanoscale structural defects in electrodeposited Ni/Al₂O₃ composite coatings. *Surf Coat Technol* 319:23–32. <https://doi.org/10.1016/j.surfcoat.2017.03.061>
- [12] Borkar T, Harimkar SP (2011) Effect of electrodeposition conditions and reinforcement content on microstructure and tribological properties of nickel composite coatings. *Surf Coat Technol* 205(17–18):4124–4134. <https://doi.org/10.1016/j.surfcoat.2011.02.057>
- [13] Gyftou P, Pavlatou EA, Spyrellis N (2008) Effect of pulse electrodeposition parameters on the properties of Ni/nano-SiC composites. *Appl Surf Sci* 254(18):5910–5916. <https://doi.org/10.1016/j.apsusc.2008.03.151>
- [14] Pinate S, Zanella C (2020) Wear behavior of Ni-based composite coatings with dual nano-SiC: graphite powder mix. *Coatings* 10(11):1060. <https://doi.org/10.3390/coatings10111060>
- [15] Walsh FC, Ponce de Leon C (2014) A review of the electrodeposition of metal matrix composite coatings by inclusion of particles in a metal layer: an established and diversifying technology. *Trans IMF* 92(2):83–98. <https://doi.org/10.1179/0020296713z.000000000161>
- [16] Tudela I, Zhang Y, Pal M, Kerr I, Cobley AJ (2014) Ultrasound-assisted electrodeposition of composite coatings with particles. *Surf Coat Technol* 259:363–373. <https://doi.org/10.1016/j.surfcoat.2014.06.023>
- [17] Watts OP (1916) Rapid nickel plating. *Trans Am Electrochem Soc* 29:395–403
- [18] Amblard J, Epelboin I, Froment M, Maurin G (1979) Inhibition and nickel electrocrystallization. *J Appl Electrochem* 9(2):233–242. <https://doi.org/10.1007/BF00616093>
- [19] Reddy A (1963) Preferred orientations in nickel electrodeposits. *J Electroanal Chem* 6(2):153–158. [https://doi.org/10.1016/S0022-0728\(63\)80152-7](https://doi.org/10.1016/S0022-0728(63)80152-7)
- [20] Nakamura Y, Kaneko N, Watanabe M, Nezu H (1994) Effects of saccharin and aliphatic alcohols on the electrocrystallization of nickel. *J Appl Electrochem* 24(3):227–232. <https://doi.org/10.1007/BF00242888>
- [21] Walsh FC, Low CTJ, Bello JO (2015) Influence of surfactants on electrodeposition of a Ni-nanoparticulate SiC composite coating. *Trans IMF* 93(3):147–156. <https://doi.org/10.1179/0020296715Z.000000000237>
- [22] Pinate S, Leisner P, Zanella C (2019) Electrocodeposition of nano-SiC particles by pulse-reverse under an adapted waveform. *J Electrochem Soc* 166:D804. <https://doi.org/10.1149/2.0441915jes>
- [23] Pinate S, Ispas A, Leisner P, Zanella C (2021) Electrocodeposition of Ni composites and surface treatment of SiC nano-particles. *Surf Coat Technol* 406:126663. <https://doi.org/10.1016/j.surfcoat.2020.126663>
- [24] Coleman S, Roy S (2014) Effect of ultrasound on mass transfer during electrodeposition for electrodes separated by a narrow gap. *Chem Eng Sci* 113:35–44. <https://doi.org/10.1016/j.ces.2014.03.026>
- [25] Crouch PC, Hendricksen HV (1983) Current efficiency on Watts baths. *Trans IMF* 61:133–140

- [26] Gyftou P, Stroumbouli M, Pavlatou EA, Asimidis P, Spyrellis N (2005) Tribological study of Ni matrix composite coatings containing nano and micro SiC particles. *Electrochim Acta* 50(23):4544–4550. <https://doi.org/10.1016/j.electacta.2004.10.090>
- [27] Pavlatou EA, Stroumbouli M, Gyftou P, Spyrellis N (2006) Hardening effect induced by incorporation of SiC particles in nickel electrodeposits. *J Appl Electrochem* 36(4):385–394. <https://doi.org/10.1007/s10800-005-9082-y>
- [28] Vaezi MR, Sadmezzaad SK, Nikzad L (2008) Electrodeposition of Ni–SiC nano-composite coatings and evaluation of wear and corrosion resistance and electroplating characteristics. *Colloids Surf A Physicochem Eng Asp* 315(1–3):176–182. <https://doi.org/10.1016/j.colsurfa.2007.07.027>
- [29] Nowak P, Socha RP, Kaisheva M, Fransær J, Celis J-P, Stoinov Z (2000) Electrochemical investigation of the codeposition of SiC and SiO₂ particles with nickel. *J Appl Electrochem* 30(4):429–437. <https://doi.org/10.1023/A:1003979117146>
- [30] Lampke T, Leopold A, Dietrich D, Alisch G, Wielage B (2006) Correlation between structure and corrosion behaviour of nickel dispersion coatings containing ceramic particles of different sizes. *Surf Coat Technol* 201(6):3510–3517. <https://doi.org/10.1016/j.surfcoat.2006.08.073>
- [31] García-Lecina E, García-Urrutia I, Díez JA, Morgiel J, Indyka P (2012) A comparative study of the effect of mechanical and ultrasound agitation on the properties of electrodeposited Ni/Al₂O₃ nanocomposite coatings. *Surf Coat Technol* 206(11–12):2998–3005. <https://doi.org/10.1016/j.surfcoat.2011.12.037>
- [32] Zanella C, Lekka M, Bonora PL (2013) Effect of ultrasound vibration during electrodeposition of Ni–SiC nanocomposite coatings. *Surf Eng* 26(7):511–518. <https://doi.org/10.1179/174329409X438961>
- [33] Tudela I, Zhang Y, Pal M, Kerr I, Cobley AJ (2015) Ultrasound-assisted electrodeposition of thin nickel-based composite coatings with lubricant particles. *Surf Coat Technol* 276:89–105. <https://doi.org/10.1016/j.surfcoat.2015.06.030>
- [34] Bérubé LP (1989) A quantitative method of determining the degree of texture of zinc electrodeposits. *J Electrochem Soc* 136(8):2314–2315. <https://doi.org/10.1149/1.2097318>
- [35] Gyawali G, Joshi B, Tripathi K, Lee SW (2017) Effect of ultrasonic nanocrystal surface modification on properties of electrodeposited Ni and Ni–SiC composite coatings. *J Mater Eng Perform* 26(9):4462–4469. <https://doi.org/10.1007/s11665-017-2891-4>
- [36] Lin CS, Huang KC (2004) Codeposition and microstructure of Nickel–SiC composite coating electrodeposited from sulphamate bath. *J Appl Electrochem* 34(10):1013–1019. <https://doi.org/10.1023/B:JACH.0000042676.26158.35>
- [37] Tudela I, Zhang Y, Pal M, Kerr I, Mason TJ, Cobley AJ (2015) Ultrasound-assisted electrodeposition of nickel: effect of ultrasonic power on the characteristics of thin coatings. *Surf Coat Technol* 264:49–59. <https://doi.org/10.1016/j.surfcoat.2015.01.020>
- [38] Lampke T, Dietrich D, Leopold A, Alisch G, Wielage B (2008) Cavitation erosion of electroplated nickel composite coatings. *Surf Coat Technol* 202(16):3967–3974. <https://doi.org/10.1016/j.surfcoat.2008.02.004>
- [39] Camargo MK, Tudela I, Schmidt U, Cobley AJ, Bund A (2016) Ultrasound assisted electrodeposition of Zn and Zn-TiO₂ coatings. *Electrochim Acta* 198:287–295. <https://doi.org/10.1016/j.electacta.2016.03.078>
- [40] Winand R (1992) Electrocrystallization—theory and applications. *Hydrometall* 29(1–3):567–598. [https://doi.org/10.1016/0304-386X\(92\)90033-V](https://doi.org/10.1016/0304-386X(92)90033-V)
- [41] Godon A, Creus J, Cohendoz S, Conforto E, Feaugas X, Girault P, Savall C (2010) Effects of grain orientation on the Hall-Petch relationship in electrodeposited nickel with nanocrystalline grains. *Scripta Mater* 62(6):403–406. <https://doi.org/10.1016/j.scriptamat.2009.11.038>
- [42] Prasad PBSNV, Vasudevan R, Seshadri SK (1992) Residual stresses of nickel electrodeposits with ultrasonically agitated bath. *J Mater Sci Lett* 11(21):1424–1425. <https://doi.org/10.1007/BF00729649>
- [43] Sanaty-Zadeh A, Rohatgi PK (2012) Comparison between current models for the strength of particulate-reinforced metal matrix nanocomposites with emphasis on consideration of Hall-Petch effect. *Mater Sci Eng A* 531:112–118. <https://doi.org/10.1016/j.msea.2011.10.043>
- [44] Zhang Z, Chen DL (2008) Contribution of Orowan strengthening effect in particulate-reinforced metal matrix nanocomposites. *Mater Sci Eng A* 483:148–152. <https://doi.org/10.1016/j.msea.2006.10.184>
- [45] Spanou S, Pavlatou EA (2011) Ni/nano-TiO₂ composite electrocoatings: correlation between structural characteristics microhardness and wear resistance. *Z Phys Chem* 225(3):313–324. <https://doi.org/10.1524/zpch.2011.0052>

Publisher's Note Springer Nature remains neutral with regard to jurisdictional claims in published maps and institutional affiliations.